OPEN

ORIGINAL ARTICLE

Mucopolysaccharidosis IIIB confers enhanced neonatal intracranial transduction by AAV8 but not by 5, 9 or rh10

JA Gilkes, MD Bloom and CD Heldermon

Sanfilippo syndrome type B (mucopolysaccharidosis IIIB, MPS IIIB) is a lysosomal storage disease resulting from deficiency of N-acetyl-glucosaminidase (NAGLU) activity. To determine the possible therapeutic utility of recombinant adeno-associated virus (rAAV) in early gene therapy-based interventions, we performed a comprehensive assessment of transduction and biodistribution profiles of four central nervous system (CNS) administered rAAV serotypes, -5, -8, -9 and -rh10. To simulate optimal earliest treatment of the disease, each rAAV serotype was injected into the CNS of neonatal MPS IIIB and control animals. We observed marked differences in biodistribution and transduction profiles between the serotypes and this differed in MPS IIIB compared with healthy control mice. Overall, in control mice, all serotypes performed comparably, although some differences were observed in certain focal areas. In MPS IIIB mice, AAV8 was more efficient than AAV5, -9 and -rh10 for gene delivery to most structures analyzed, including the cerebral cortex, hippocampus and thalamus. Noteworthy, the pattern of biodistribution within the CNS varied by serotype and genotype. Interestingly, AAV8 also produced the highest green fluorescent protein intensity levels compared with any other serotype and demonstrated improved transduction in NAGLU compared with control brains. Importantly, we also show leakage of AAV8, -9 and -rh10, but not AAV5, from CNS parenchyma to systemic organs. Overall, our data suggest that AAV8 represents the best therapeutic gene transfer vector for early intervention in MPS IIIB.

Gene Therapy (2016) 23, 263–271; doi:10.1038/gt.2015.111

INTRODUCTION

Mucopolysaccharidosis IIIB (MPS IIIB) is a lysosomal storage disease, which results from a deficiency in N-acetyl-glucosaminidase activity and manifests around 5 years of age. Clinical signs include hyperactivity, loss of social interaction and progressive mental degeneration, which eventually results in severe impairment of neurocognitive ability and loss of motor function.[1,2] Death often occurs between the ages of 15 and 20 years. The well-characterized MPS IIIB mouse model has been utilized to test therapeutic interventions and possesses many of the same biochemical, histological and clinical features as the human disease.[3,4] There is currently no cure for MPS IIIB.

Gene therapy has great potential for treating lysosomal storage diseases; however, widespread gene delivery throughout the central nervous system (CNS) remains a major challenge due to the need to overcome the blood brain barrier. The recombinant adeno-associated virus (AAV) vector system has been a favored gene delivery tool, and has proven highly efficient in transducing post-mitotic cells in a wide range of tissues, including the CNS. Further, no significant pathogenesis has been linked to AAV in humans. Direct administration of rAAV viral vectors into brain parenchyma can serve to bypass the blood brain barrier, thereby allowing targeted transduction of neuronal cells. Indeed, successful AAV-mediated gene therapy has been demonstrated in MPS models,[5–9] which resulted in improvements in neuropathology, behavior and increased lifespan. However, differential responses are observed based on the serotype of AAV that is administered and age at vector administration.[10–16] Several studies suggest that the greatest therapeutic advantage would stem from early treatment intervention, before disease pathology becomes evident and irreversible.[17–20]

Viral vector transduction is modulated by the presence and distribution of cell-surface receptors. Thus, neuronal cell tropism can be dictated by pseudotyping AAV vectors with capsid proteins from different serotypes. To date, several new AAV serotypes have been cloned[21,22] and allow packaging of the AAV2 vector backbone.[21,23] In this study, we examined the transduction patterns of pseudotyped AAV vectors with capsids from AAV serotypes -5, -8, -9 and -rh10, each having demonstrated proficiency in neuronal cell transduction.[14,18] Several studies suggest an age-dependent phenomenon for transduction patterns,[16,17,19,24] with rapid brain development possibly facilitating vector biodistribution. We therefore compared transduction patterns after CNS intra-parenchymal injection in the rapidly developing neonatal mouse brain to determine which serotype yields the most efficacious outcome in transduction and biodistribution patterns. We anticipate these results will guide clinical approaches in determining the most effective gene therapy vector for age-dependent treatment of MPS IIIB.

RESULTS

Serotype- and genotype-dependent differences in general rAAV-green fluorescent protein biodistribution and expression

Since widespread vector biodistribution would facilitate global CNS transduction, we first sought to assess and quantify overall rAAV-green fluorescent protein (GFP) biodistribution within the CNS after intracranial six-site vector delivery (Figure 1a). Three months post injection of AAV5, -8, -9 and -rh10, four spatially
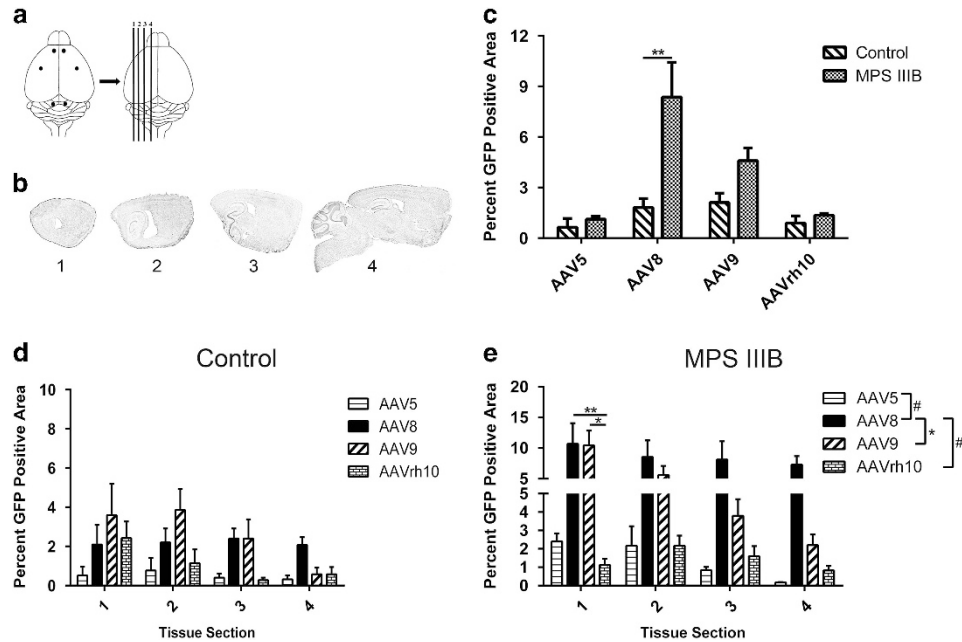
Department of Medicine, University of Florida, Gainesville, FL, USA. Correspondence: Dr CD Heldermon, Department of Medicine, University of Florida, 1600 SW Archer Road, Campus Box 100277, Gainesville, FL 32608, USA.
E-mail: coy.heldermon@medicine.ufl.edu

Figure 1. AAV serotype-dependent general CNS biodistribution. Following six site-directed vector administration (**a**), representative tissue sections of interest (**b**) were analyzed for percentage of area with GFP expression. Differences in combined percentage GFP area for all four sections were quantified for each serotype based on genotype (**c**), and rAAV-GFP expression was quantified for each selected brain section by serotype in 3-month-old control (**d**) and MPS IIIB littermates (**e**). Two-way ANOVA was used to assess differences within tissue section based on serotype, and one-way ANOVA was used to test individual differences between serotype, $n = 3$–6/cohort *$P < 0.05$; **$P < 0.01$. Data represented as mean ± s.e.m.

distinct and relatively equidistant areas were selected for quantitative assessment of GFP expression. Using the Allen Brain Atlas, we estimated the relative anatomical locations, in millimeters, medial to lateral, − 4.2, − 3.72, − 2.72 and − 1.72 (Figure 1b). The overall percentage of GFP-positive area for all four sections was compared between control and MPS IIIB cohorts for each serotype (Figure 1c). We observed a marked increase in transduction area for AAV8-treated MPS IIIB animals compared with controls ($P < 0.01$), but no significant differences were observed for AAV5, -9 or -rh10. Variation was significantly affected by the interaction between AAV serotype and genotype for AAV8. The percentage of GFP-positive area was also compared for each serotype in each of the four represented sections within control and MPS IIIB cohorts (Figures 1d and e). In both cohorts, all vectors exhibited spread to each of the four tissue sections investigated, with AAV8 and to a lesser degree, -9, being predominant. In the control cohort, no statistically significant difference was achieved favoring any serotype between or within sections (Figure 1d). In the MPS IIIB-treated cohort, the trend showed that the largest percentage of GFP-positive area was exhibited by AAV8, ranging from approximately 10% in section 1 down to 8% in section 4, although significant differences among serotypes were achieved only in section 1 (Figure 1e). Cumulative comparisons of all sections, however, revealed that AAV8 had a significantly greater area of GFP expression than -5 ($P < 0.001$), -9 ($P < 0.05$) and -rh10 ($P < 0.001$) with no other significant serotype differences (Figure 1e, legend). This marked difference in AAV8 expression may suggest a difference in regulatory mechanisms modulating AAV8 transduction between these two genotypes. Further, in the MPS IIIB group, AAV9 biodistribution and expression levels were higher, though not significantly, compared with control, although AAV5 and -rh10 transduction was equivalent between genotypes. These observations suggest that the biodistribution and localization preferences of AAV vectors may be modulated as a consequence of the health of the subject and the composition of the extracellular milieu.

Genotype-specific biodistribution patterns in mid-sagittal cortex, hippocampus, thalamus and cerebellum

Given the unique functions attributed to certain structural areas of the brain, we next sought to assess for differences in AAV-GFP localization within mid-sagittal brain sections. Comparative assessment of GFP expression patterns in focal CNS regions revealed that AAV5 GFP expression was heavily localized within ependymal cells, consistent with previous findings,[13] and otherwise exhibited diffuse and punctate distribution patterns, primarily in somatomotor layers V and VIa of the frontal cortex in both control and MPS IIIB mice (Figure 2a). In the MPS IIIB cohort, we observed higher levels of transduction in the forebrain, midbrain and hindbrain regions of AAV8-treated animals. Noteworthy areas include the cortex and to a lesser degree the hippocampus and thalamus. This trend was somewhat similar for AAV9, although the robustness of GFP transduction appeared substantially diminished. The cerebellum was minimally transduced by all serotypes. Control animals exhibited similar patterns of staining in the cortex, but there was less overall vector biodistribution and there were notable differences in GFP expression in the inferior and superior colliculus (Figure 2a).

As the cortex, hippocampus, thalamus and cerebellum have important roles in reasoning, memory, signal relay and motor coordination, respectively, we sought to quantitate the abundance of GFP as a consequence of AAV serotype in each of these specific regions at the mid-sagittal slice (Figure 2b). For these regions, noticeable differences in GFP biodistribution were primarily evident in the cortex for MPS IIIB and control, and marginally in the hippocampus for control animals. In the control group, AAV8 demonstrated greater expression area in both the cortex and the hippocampus (Figure 2c, $P < 0.001$ vs -5 and -rh10 in cortex and $P < 0.05$ vs -5, -9 and -rh10 in the hippocampus). In the MPS IIIB group, no significant difference in GFP expression area was observed in the hippocampus, thalamus or cerebellum. However, in the MPS IIIB cortex, AAV8 demonstrated robust GFP
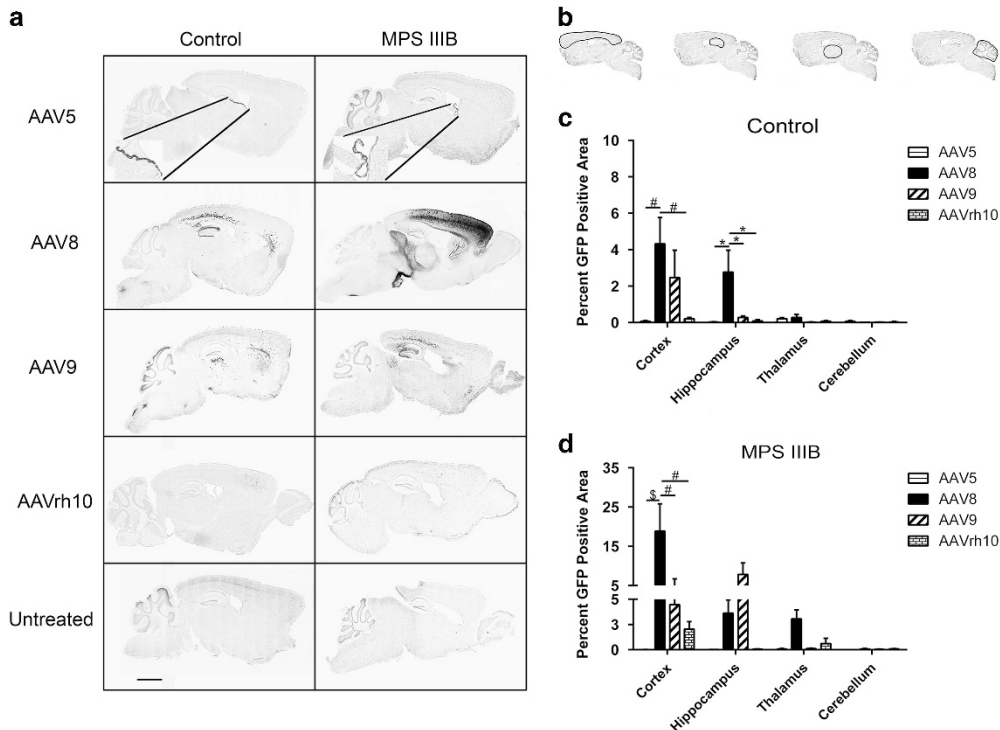
Figure 2. Mid-sagittal AAV serotype-dependent regional biodistribution. Mid-sagittal brain sections of control and MPS IIIB 3-month-old littermates were assessed for the presence of **r**AAV-GFP (dark areas, scale bar = 2mm). Insets in AAV5 panels reflect transduced ependymal cells at ×20 magnification (**a**). Percentage area of GFP expression was assessed in the cortex, hippocampus, thalamus and cerebellum, outlined in (**b**) respectively of control (**c**) and MPS IIIB animals (**d**). All sagittal sections were scanned at ×20 magnification, and GFP expression was quantified using Aperio ImageScope algorythm. Two-way ANOVA was used to assess differences within each region based on serotype, and one-way ANOVA was used to test individual differences between serotype, $n = 3$–6/cohort, *$P < 0.05$, #$P < 0.001$, $P < 0.0001$. Data represented as mean ± s.e.m.
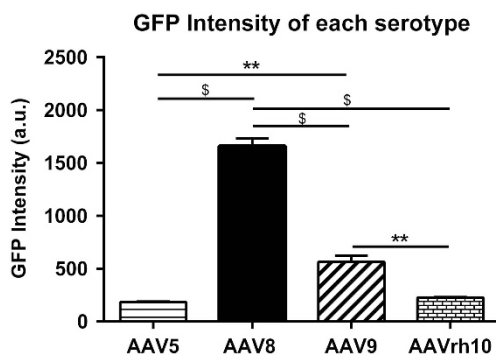

Figure 3. rAAVs exhibit differences in GFP production in MPS IIIB brain as indicated by resulting GFP intensity. Mid-sagittal sections of 3-month-old MPS IIIB animals were used to quantitate intensity of AAV-based GFP production. GFP intensities in the cortex, hippocampus, thalamus and cerebellum of each animal were summed. Data were analyzed by one-way ANOVA. **$P < 0.01$, $P < 0.0001$. Data represented as mean ± s.e.m., $N = 3$/serotype.

expression compared with all other vectors ($P < 0.0001$ for AAV5 and $P < 0.001$ for -9 and rh10, respectively, Figure 2d).

Use of AAV8 results in robust production of GFP

The observation that AAV8 and to a lesser degree AAV9 exhibited the highest degree of biodistribution in MPS IIIB animals compared with healthy control animals, prompted us to continue assessment of these serotypes in the MPS IIIB group moving forward. Since we also observed qualitative differences in the

robustness of GFP expression based on serotype, we conducted a quantitative assessment of GFP intensity by near infrared analysis using the Odyssey instrument. The advantage of using this system is that it offers increased sensitivity and more accurate detection of both strong and weak signals over a broader linear dynamic range. Using mid-sagittal brain sections of MPS IIIB animals, the cumulative GFP intensity within the cortex, hippocampus, thalamus and cerebellum was quantitated for the different serotypes (Figure 3). Consistent with qualitative observations, we show that use of AAV8 resulted in superior and robust expression of GFP ($P < 0.0001$ vs -5, -9 and rh10). We also noted that AAV9 expressed higher GFP intensity compared with -5 and -rh10 ($P < 0.01$ for both). AAV5 and -rh10 were comparably inferior. These data indicate that use of AAV8 in MPS IIIB animals is most likely to yield the greater protein production in these regions when compared with AAV5, -9 and -rh10.

rAAVs preferentially transduce neurons and astrocytes in MPS IIIB mice

To determine whether specific cell type transduction preference is displayed by any of the rAAVs, we investigated four different types of neuronal cells: neurons (NeuN), astrocytes (glial fibrillary acidic protein, GFAP), microglia (ionized calcium-binding adapter molecule 1, Iba1) and oligodendrocytes (oligodendrocyte-specific protein, OSP). The phenotype of transduced cells in the cortex of mid-sagittal sections was determined based on the presence of GFP co-localized with cell-specific markers (Figure 4). All serotypes transduced both astrocytes and neurons, but not microglia or oligodendrocytes. Noteworthy, the data suggest that the robustness of GFP expression in astrocytes and neurons differed by serotype. It also appeared that AAV9 exhibited a preference for
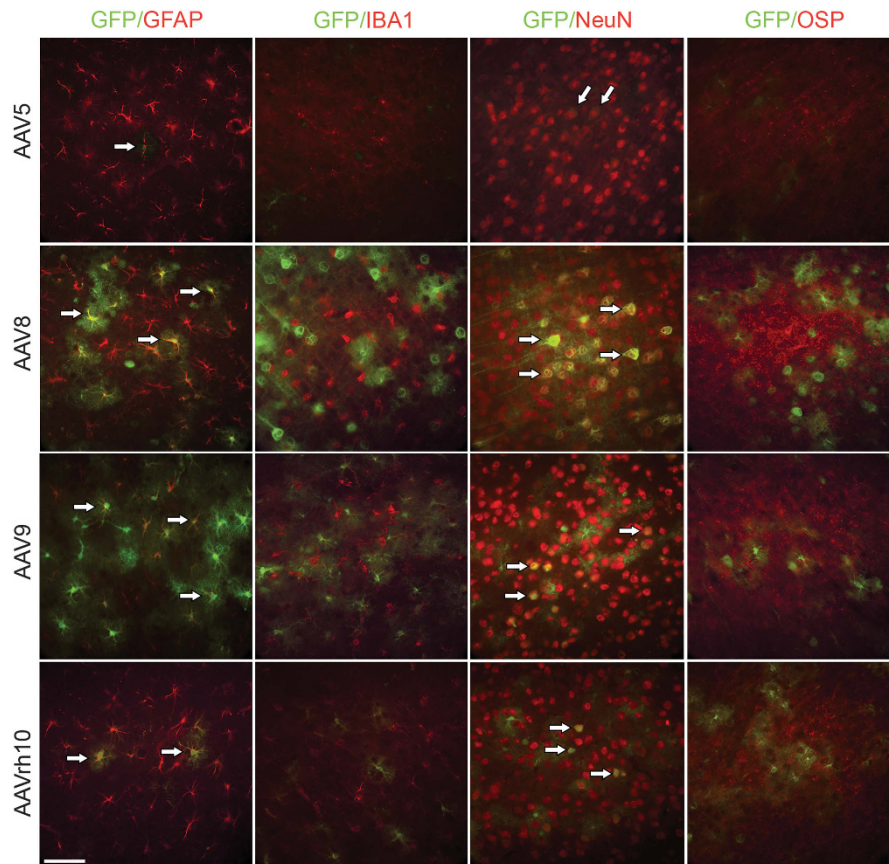
Figure 4. All AAV serotypes transduce neurons and astrocytes but not microglia and oligodendrocytes in the cortex. Representative cortical images of AAV5, -8, -9 and -rh10 transduced MPS IIIB animals stained for neurons (NeuN), astrocytes (GFAP), microglia (Iba1) and oligodendrocytes (OSP). Arrows indicate areas of co-localization of each cell type and rAAV-GFP in the cortex of MPS IIIB animals. Images taken with ×40 objective lens, scale bar = 60 μm.

astrocytes, while AAV8 preferred neurons. Although both AAV5 and -rh10 transduced astrocytes and neurons, the robustness of transduction was considerably diminished, particularly in AAV5, compared with -8 and -9. Taken together, these data reflect the selective difference in cell type-specific transduction, possibly as a consequence of differential receptor expression.

Variable cortical expression levels of GFP in MPS IIIB animals are observed among different AAV serotypes

We next attempted to assess differences in serotype-dependent expression efficiency in two different neuronal cell types, neurons and astrocytes. We selected between 150 and 200 neurons and astrocytes subjectively assessed to have representation of both low and high GFP expression from the cortex of MPS IIIB mice transduced with each serotype. Transduced cells were assessed using the Positive Pixel Count FL v1 algorithm within ImageScope. All images were analyzed at the same exposure. For AAV5- and AAVrh10-treated animals, we utilized a lower intensity threshold value which increased the sensitivity of the algorithm to detect very low levels of GFP expression (intensity minimum = 0.1 and intensity maximum = 1) (Figure 5). Our data revealed serotype-dependent differences in the robustness of GFP expression between neurons and astrocytes. In AAV5- and AAV9-treated animals, the resulting GFP intensity levels suggested that astrocytes were higher expressing compared with neurons ($P < 0.0001$ and $P < 0.01$, respectively). Whereas, in AAV8- and AAVrh10-treated animals, neurons were higher expressing ($P < 0.0001$ and $P < 0.01$, respectively). Our data reveal

serotype-dependent and cell type-specific differential transduction profiles within the CNS of MPS IIIB animals.

CNS administration of rAAV also results in somatic biodistribution

To determine whether CNS administered rAAVs would also facilitate somatic transduction, we tested various organs including the heart, liver, muscle, kidney and spleen of AAV5-, AAV8-, AAV9- and AAVrh10-treated control and MPS IIIB-treated animals. Interestingly, we saw that AAV8, -9 and to a lesser extent, -rh10 robustly transduced the cardiac myocytes and the liver. Muscle, kidney and spleen tissue transduction was not observed for any serotype (Figure 6). Although CNS treatment with AAV8, -9 and -rh10 resulted in somatic transduction of some organs, AAV5 did not result in any noticeable transduction of any organs tested.

DISCUSSION

In this study, we comprehensively tested four AAV serotypes in the MPS IIIB mouse brain to assess tropism and transduction outcomes after neonatal intracranial six site-directed vector delivery. For many neurological diseases including MPS III, treatment during infancy will be necessary to prevent irreversible brain injury. As timing of injection is crucial, we chose to inject at postnatal day 3 to facilitate vector biodistribution within the brain. Each of the four vector serotypes used in this study was constructed with the humanized green fluorescent protein cassette driven by the chicken beta-actin promoter and cytomegalovirus enhancer elements flanked by AAV2 inverted terminal repeats. Therefore, any differences in biodistribution, transduction
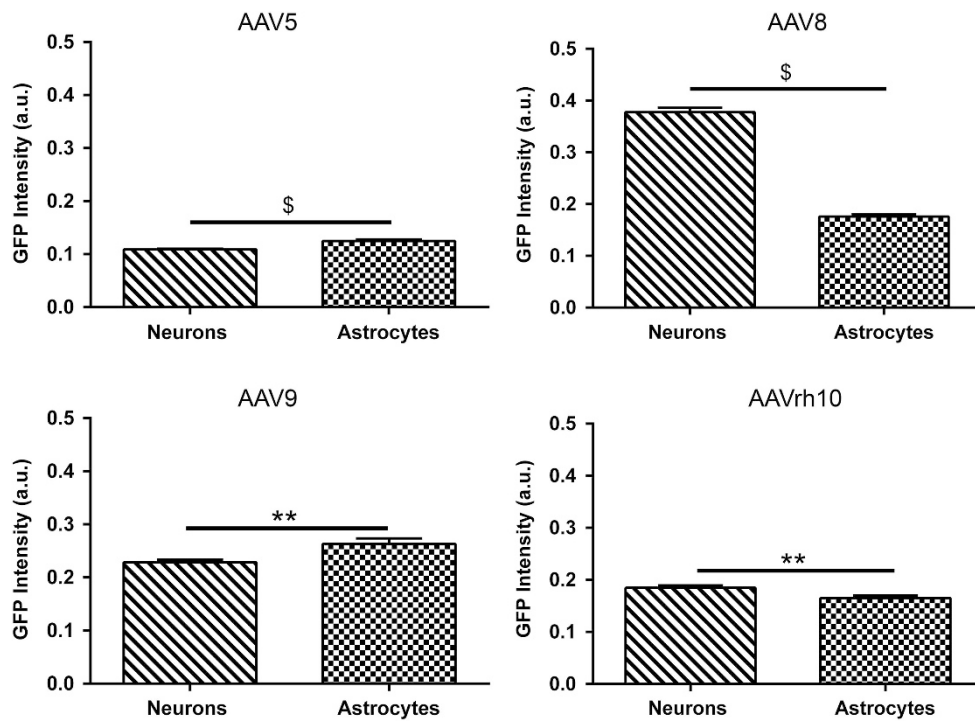
Figure 5. Differences in GFP intensity of transduced cells are observed based on AAV serotype. GFP intensity of AAV transduced neurons and astrocytes was assessed in MPS IIIB animals at 3 months of age. Serotype-dependent differences in GFP intensity were determined using APERIO ScanScope FL Positive Pixel Count FL algorithm and quantitated using Student's *t*-test. $N = 3$/serotype, **$P < 0.01$, $^{\$}P < 0.0001$. Data represented as mean ± s.e.m.
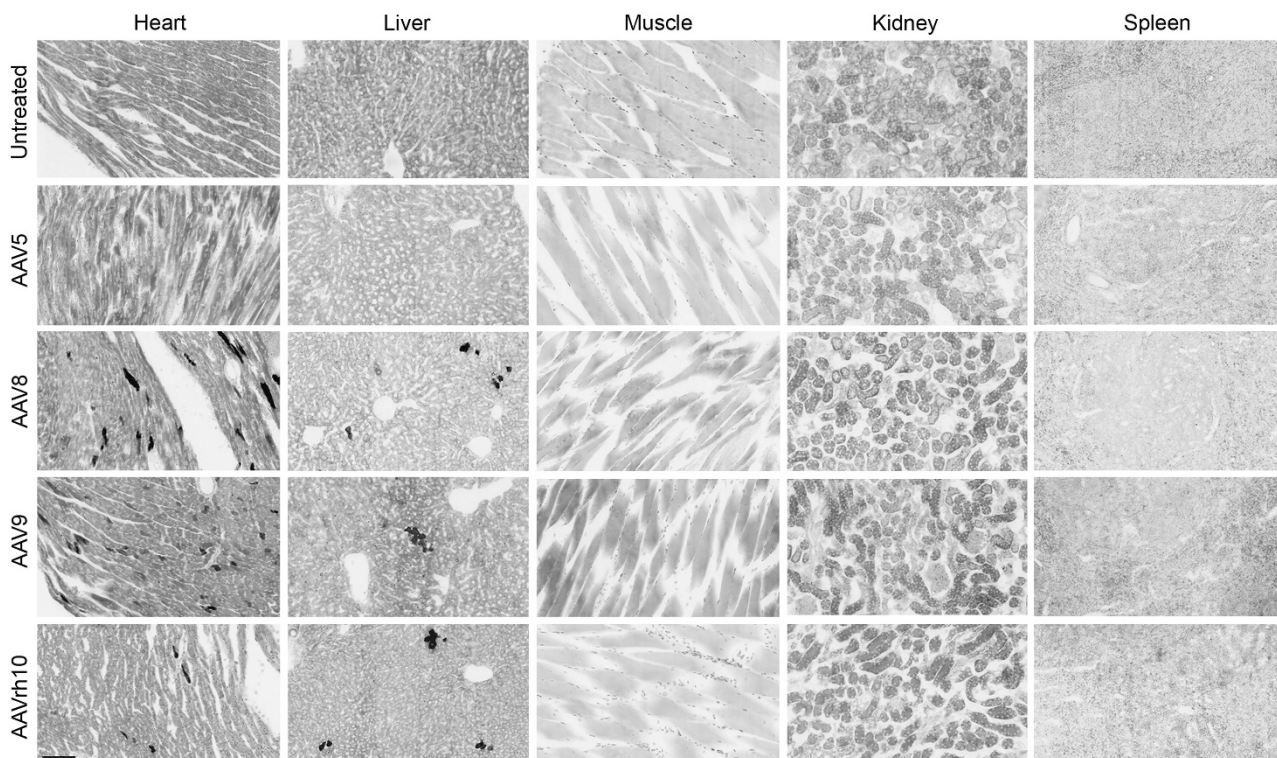

Figure 6. CNS administered rAAVs also foster differential somatic transduction. Representative organs of 3-month-old control and MPS IIIB-treated animals were tested for somatic transduction of rAAV-GFP in the heart, liver, muscle, kidney and spleen. The presence of rAAV-GFP is indicated by black areas in each tissue section. All tissue sections were scanned at ×20 magnification, scale bar = 100 μm.

and GFP intensity are directly attributable to variations in capsid amino-acid composition and respective differences in receptor tropism for each serotype. To date, primary and/or co-receptors have been described for AAV5 and -9. Co-receptor but not primary receptor has been identified for AAV8. Neither primary nor co-receptors have been described for AAVrh10.[25] The observable similarities and differences in transduction and biodistribution profiles among the different serotypes may be partly explained by the fact that AAV8 and -9 share 84% sequence homology in their capsid amino acids; whereas AAV5 only shares 57% homology with AAV8 and 55% homology with AAV9.[26] Differences in capsid structure and receptor affinity of AAVrh10 are also expected to have a central role in modulation of its cellular interaction.

In our disease model, serotype- and genotype-dependent differences in biodistribution and transduction profiles of each rAAV were observed. The largest cumulative percentage of GFP-positive area was achieved by AAV8 in the MPS IIIB model, suggesting that disease state may affect vector efficiency. We also observed differences in biodistribution trends of the different serotypes. Notably, with the exception of AAV8, the trend suggests diminishing levels of GFP expression from lateral to medial sections in all other serotypes. Overall, AAV8 and -9 appear to be superior in MPS IIIB animals compared with control, whereas AAV5 and -rh10 are comparably unimpressive in both genotypes (Figure 1). Interestingly, the differential activity of AAV9 between normal and diseased states for MPS VII was previously reported. This difference was determined to be due to increased sialic acid levels in the MPS VII brain interfering with AAV9 transduction,[27] once again making the case for the interplay of factors related to disease pathophysiology in the modulation of AAV activity. Although we cannot exclude minor differences in injection site variation, we learned that the spread of most serotypes, except AAV8 in the MPS IIIB group, was somewhat limited in range, primarily being localized within the cortex, with some trafficking to the hippocampus and thalamus. We also observed robust GFP transduction in AAV8-treated animals compared with control, although this difference was not obvious in other serotypes. Interestingly, AAV5, but not -8, -9 or -rh10, demonstrated robust transduction of ependymal cells but poor transduction in other regions. Similar tropism preferences for ependymal cells were observed by AAV9 after intrathecal administration in a non-human primate model.[28] Although these studies utilized different injection sites, the observations support the notion that a species-specific analysis of AAV may be warranted when assessing for therapeutic potential. These differences in efficiency may further be explained as a consequence of tropism preferences and receptor availability, differential susceptibility to proteases or other undetermined factors. Noteworthy, there was not a substantial transduction of the cerebellum by any serotype (Figure 2).

Since our primary interest is in determining the best serotype of AAV to use for disease modulation in MPS IIIB and the highest degree of vector biodistribution occurred in the MPS IIIB disease model, with AAV8 in particular, we further conducted the remainder of studies focusing on the MPS IIIB model. We examined the overall difference in intensity levels of GFP production based on AAV serotype in specific regions of the mid-sagittal brain. We observed significantly higher GFP intensity levels in these regions of MPS IIIB animals treated with AAV8, compared with AAV5, -9 and -rh10. These data suggest that AAV8 exhibits enhanced efficiency of cellular transduction, and intracellular trafficking compared with its counterparts, ultimately resulting in improved protein production (Figure 3).

To further understand tropism preferences of these serotypes within the MPS IIIB brain, we analyzed astrocytes, microglia, neurons and oligodendrocytes. We observed that all serotypes transduced neurons and astrocytes, although to varying degrees, but no serotype transduced microglia or oligodendrocytes

(Figure 4). Since microglia undergo high turnover in the CNS, lasting gene expression could be impaired. Alternately, these viruses may simply be unable to transduce these specific cell types well. Previous studies have shown that microglial expression was only achieved using specialized promoters, which suggests that the lack of microglial GFP expression may be a consequence of inefficient transcription of the insert by the microglial machinery.[29]

To understand why there appeared to be variations in intensity of GFP transduced neurons and astrocytes, we assessed rAAV transduced cell types for differences in GFP intensity levels. We observed serotype-dependent cell type tropism preferences. Both AAV8 and -rh10 transduced neurons with higher efficiency as indicated by higher GFP intensity levels, while AAV5 and -9 transduced astrocytes more efficiently (Figure 5). Such cell type-specific preferences may be attributed to differences in expression of cell-surface receptors for AAV vectors, while low astrocytic transduction may be a consequence of lost genomes during glial expansion, a hallmark of MPS IIIB referred to as astrogliosis. The presence of astrocytic transduction by AAV8, -9 and -rh10 in the MPS IIIB model, is in contrast to that observed in the MPS VII model, as previously demonstrated.[30] This suggests that the differences in storage products in MPS VII may be modulating AAV astrocyte transduction efficiency. This also suggests that tropism is likely to be influenced differently for each disease state. In the cerebellum, few purkinje cells were transduced by any serotypes, possibly suggesting overall low AAV-specific receptor abundance at this early time point.

It can be speculated that excess heparan sulfate or possibly other cell components found at high levels, such as gangliosides, in the MPS IIIB cellular environment may be responsible for differentially regulating vector biodistribution. With the exception of Bovine AAV, little is known about the role of gangliosides in the modulation of AAV transduction.[31] It is conceivable that accumulation of heparan sulfate, gangliosides or other secondarily elevated products in MPS IIIB animals may be facilitating the interaction of different AAVs with their host cells.

Although alternative explanations of differences in dilution, starting titer and packaging efficiency might be hypothesized, none of these would be expected to be evident only in the AAV8-treated MPS IIIB versus unaffected control animals, as both genotypes were present in the same litter and treated with the same vector stock. Similarly, all vector stocks were produced by the same vector core and concentrations determined by the same method.

The implications of differences in serotype transduction efficiency for CNS-directed AAV-based gene therapy treatment goes beyond correction of neuronal aberrations associated with MPS III. Any CNS disease that changes the distribution of extracellular milieu components may alter the usual vector distribution and efficiency. For example, the overall relatively poor performance of -rh10 in our MPS IIIB model is in contrast to studies in the LINCL mouse model by Sondhi et al.,[32] which revealed that administration of AAVrh10CLN2 lead to superior CNS biodistribution and significant correction of disease pathology compared with AAV5CLN2 and AAV8CLN2. This makes disease specific, and indeed species specific, assessments of these vectors very important for clinical development. The differential capacity of rAAV serotypes to transduce large numbers of neuronal cells in different regions may be relevant for treating neurological diseases with a large loss of neurons such as Tay-Sachs, many mucopolysaccharidoses with neurological involvement and neuronal ceroid lipofuscinoses.[32–34] Furthermore, differences in transduction of astrocytes by rAAVs expressing secreted neurotrophic factors may be beneficial for a number of neurodegenerative diseases with astrocyte atrophy or deficiencies such as Amyotrophic Lateral Sclerosis and Alzheimer's disease.[35,36]

Finally, we noted serotype-dependent differences in systemic tissue transduction. AAV9 has been broadly hailed for its ability to cross the blood brain barrier, and AAV8 has more recently demonstrated this capacity. In our experiments, we observe that this capacity is not exclusively in a systemic to CNS direction but also from the brain to the circulation. We observed this trans-BBB passage also to a lesser extent for AAVrh10. It can be postulated that rAAVs exited the CNS and gained systemic entry by accessing the arterial supply. Systemic presence was most pronounced in the heart, primarily mediated by AAV8. The presence of AAV8 and -9 was observed in the heart and liver, but surprisingly, not in skeletal muscles (Figure 6). Several reports of AAVs crossing from systemic circulation to the CNS have been made.[37–39] Noteworthy, a recent study by Ribera *et al.*[40] also demonstrated systemic leakage of NAGLU-coding AAV9 from cerebrospinal fluid to the liver, leading to whole body disease correction.[40] Additionally, liver directed CNS leakage has been reported in an MPS IIIA model after intracerebrospinal administration.[34] However, to our knowledge, this is the first report of systemic leakage of AAV8, -9 and -rh10 from the CNS parenchyma in the MPS IIIB model and AAV8 or -rh10 in any published model. We did not observe any systemic transduction by AAV5, suggesting a difference in transport machinery.

In summary, we have demonstrated that CNS-directed infusion of different AAV serotypes into neonatal animals results in differential patterns of AAV transduction and biodistribution between MPS IIIB and unaffected control animals. We show that AAV8 yielded superior results both in transduction and in biodistribution profiles in MPS IIIB animals compared with other serotypes, and also facilitated robust somatic transduction of the heart and liver. Our data suggest that AAV8 is the preferred candidate for early intervention in gene therapy-based treatment of this disease.

Since the unique environment of the CNS would facilitate long-term therapeutic transgene expression, delivering a high expressing promiscuous AAV vector capable of transducing numerous neuronal cell types through a minimally invasive method would be the ideal therapeutic outcome. In recent studies, capsid-modified variants of AAVs have shown great potential in increasing transduction efficiency.[41–43] In one study using a single tyrosine capsid-modified variant of AAV8, an increase in hepatic gene transfer was noted.[44] Our next steps are to determine whether capsid-modified variants of AAV8 will confer any therapeutic advantage in transgene expression in the MPS IIIB model; as well as, to identify a method of vector administration that would facilitate global CNS delivery. Future steps are to deliver therapeutic NAGLU to MPS IIIB animals using an AAV8-based vector and explore mechanisms for the observed transduction differences in MPS IIIB compared with unaffected animals.

MATERIALS AND METHODS

AAV constructs
Recombinant AAV2 plasmids pseudotyped with capsid proteins from AAV5, -8, -9 and -rh10 were produced, purified and titered at the University of Florida Powell Gene Therapy Center Vector Core Laboratory (Gainesville, FL, USA). Vector titer was determined by dot blot assays,[45] and final aliquots were resuspended in balanced salt solution (BSS, Alcon Laboratories, Fort worth, TX, USA). Each of the four rAAV (AAV-2/5, -2/8, -2/9, -2/rh10) constructs express humanized green fluorescent protein driven by the hybrid cytomegalovirus enhancer/chicken beta-actin promoter.

Animals and IC6-based vector administration
The congenic C57BL/6 NAGLU-deficient mouse strain was a kind gift from Elizabeth Neufeld (University of California Los Angeles, CA, USA) by way of Mark Sands (Washington University, St. Louis, MO, USA), and was

maintained and expanded by strict sibling mating.[3] Wild-type (+/+), heterozygous (−/+) (subsequently referred to as 'Control') and mutant (−/−) MPS IIIB genotypes were determined by PCR of NAGLU exon 6 and the neomycin insertion or by NAGLU-4-methylumbelliferone enzyme assay[46] on tissue samples from newborn mice. All animal studies were performed in accordance with guidelines of the University of Florida Institutional Animal Care and Use Committee. Intracranial rAAV treatment of control and MPS IIIB animals from the same litter was performed as previously described.[20,47] All treatments were performed in genotyped pups at 3–4 days of age, with the same serotype used for littermates and were well tolerated. Between three and six animals per AAV serotype were utilized. This range was appropriate based on numbers from prior similar studies in other models for CNS distribution.[13,15] Intracranial rAAV-GFP was administered by six direct injections per mouse of 2 µl each at a concentration of 1.4×10^{12} vector genomes/ml into the bilateral frontal (from bregma: 2 mm lateral and 1 mm posterior, 1.5 mm deep), temporal (from bregma: 3 mm lateral and 3 mm posterior, 2.5 mm deep) and cerebellar (from lambda: 1 mm lateral and posterior, 1.5 mm deep) regions using a 32-gauge Hamilton syringe (Narishige Int., East Meadow, NY, USA). From the intention-to-treat animals, two AAV5-, one AAV8-, one AAV9- and one AAVrh10-treated animals exhibited evidence of vector extrusion during injection and were thereafter excluded from analysis and are not used for any part of this publication. For the animals used in this publication, unless otherwise indicated, three MPS IIIB and four control mice were AAV5 treated, six MPS IIIB and control mice were AAV8 and AAV9 treated, respectively, and four MPS IIIB and five control mice were AAVrh10 treated. Neonates were cryoanesthetized before treatment and were then placed on a warming pad after treatment, before being returned to their mothers.

Histological procedures
Three months after treatment, animals were killed and tissue was harvested for histological assessment. Initially, mice were killed with 800 µl of Ketamine (120 mg/kg)/Xylazine (16 mg/kg) cocktail followed by thoracotomy before transcardial perfusion with PBS followed by ice-cold 4% paraformaldehyde. Brains were extracted and post-fixed for 4 h at 4 °C, followed by overnight incubation in 20% sucrose in PBS at 4 °C. Brains were subsequently embedded in O.C.T medium (Triangle Biomedical Sciences, Durham, NC, USA) and rapidly frozen in a 2-methyl-butane/dry ice bath. Sagittal serial sections were cut to a thickness of 20 µm and stored in a cryoprotective solution at − 80 °C until use.

Immunofluorescence
To determine the phenotype of GFP-positive cells, tissue sections were incubated with neuron-specific nuclear protein (NeuN; neuronal marker), GFAP (astrocyte marker), Iba1 (microglia marker) and OSP (oligodendrocyte marker) primary antibodies. Free floating sections were washed in 1× PBS/0.01% Triton X-100, then 1× PBS followed by blocking with 2% normal goat serum (Vector Laboratories, Burlingame, CA, USA; Cat. #: 5425 S) in 1× PBS for 1 h at room temperature. Sections were incubated overnight at 4 °C with NeuN (1:500; EnCor Biotechnology, Gainesville, FL, USA; Cat. #: MCA-1B7), GFAP (1:500; Abcam, Cambridge, MA, USA; Cat. #: ab7260), Iba1 (1:500; WAKO, Richmond, VA, USA; Cat. #: 019-19741) and OSP (1:500; Abcam; Cat. #: ab53041). The following day sections were washed at room temperature with PBS/0.01% Triton X-100, followed by 1× PBS. Secondary antibodies Alexa Fluor 594 anti-mouse (1:750 to visualize NeuN; Molecular Probes, Eugene, OR, USA; Cat. # A11005) or Alexa Fluor 594 anti-rabbit (1:750 to visualize GFAP, Iba1 or OSP; Molecular Probes; Cat. #: A11012) were added in the presence of 2% normal goat serum in 1× PBS and incubated for 1 h at room temperature. Sections were subsequently mounted to slides and counterstained with DAPI (4,6-diamidino-2-phenylindole, Vector Laboratories; Cat. #: H-1200). Slides were analyzed on a Zeiss Axioplan 2 upright fluorescent microscope (Carl Zeiss Jena GmbH, Jena, Germany) equipped with appropriate filters. Images were captured with a QImaging Retiga 4000R monochrome camera (QImaging Corporation, Surry, BC, Canada) and MetaVue software version 6.2r4 (Molecular Devices, Downingtown, PA, USA). Compositions of ×40 pictures were prepared using Photoshop CS6 (Adobe, San Jose, CA, USA).

Quantitation of GFP
To quantify the GFP-positive area, automated whole-section imaging was done using the Scanscope FL (Aperio Technologies, Vista, CA, USA), which consisted of an 8/10-bit monochrome TDI line-image capture

camera. Analysis was done with accompanying ImageScope software (Aperio Technologies, Vista, CA, USA). For fluorescent-based quantitative assessment of GFP, total GFP percentage per brain section was assessed using the Positive Pixel Count FL v1 algorithm within ImageScope. Intensity thresholds were set at a minimum, between 0.1 and 0.2, and at a maximum of 1. To determine fluorescent-based GFP intensity based on cell type, the minimum intensity threshold was set to 0.1 for AAV5 and -rh10 and 0.3 for AAV8 and -9. Regions of interest were demarcated using the Allen Reference Atlas as a neuroanatomical reference. GFP-positive area was determined using the average from three independent tests performed by three readers in a blinded manner.

To more reliably assess differences in GFP intensity as a consequence of AAV serotype, the Odyssey Infrared Imaging system (Model #: 9120, Li-Cor Bioscience, Lincoln, NE, USA) was utilized. Briefly, mid-sagittal brain sections of AAV5-, AAV8-, AAV9- and AAVrh10-treated MPS IIIB animals were incubated overnight with a GFP antibody (1:2000, Abcam; Cat. #: ab290) in $1 \times$ PBS/0.01% TBS-T/10% NDS/1% BSA buffer. To visualize GFP, donkey anti-rabbit 680 DR was used (1:5000, Li-Cor Bioscience; Cat. # 926-68073). Sections were then mounted to slides and allowed to dry overnight followed by clearing with Xylene. Sections were again air dried overnight and analyzed using the Odyssey system the following day.

Statistical analysis

GraphPad Prism 6 (GraphPad Software, La Jolla, CA, USA) was used for statistical analysis. Two-tailed Student's t-test was used for unpaired data. Brown-Forsythe test was performed to confirm equal variance, and Tukey's test was used to correct for multiple comparisons for ANOVA. For comparisons with unequal variance, a log transform was used to normalize the data and reduce heterogeneity. Bar graphs are shown as mean ± s.e.m. Probability $P < 0.05$ was considered as statistically significant.

CONFLICT OF INTEREST

The authors declare no conflict of interest.

REFERENCES

1 Yogalingam G, Hopwood JJ. Molecular genetics of mucopolysaccharidosis type IIIA and IIIB: diagnostic, clinical, and biological implications. *Hum Mutat* 2001; **18**: 264–281.

2 Gilkes J, Patterson B, Heldermon C, Mucopolysaccharidosis III. Molecular genetics and genotype-phenotype correlations. *OA Genet* 2014; **2**: 1.

3 Li HH, Yu W-H, Rozengurt N, Zhao H-Z, Lyons KM, Anagnostaras S et al. Mouse model of Sanfilippo syndrome type B produced by targeted disruption of the gene encoding alpha-N-acetylglucosaminidase. *Proc Natl Acad Sci USA* 1999; **96**: 14505–14510.

4 Heldermon CD, Hennig AK, Ohlemiller KK, Ogilvie JM, Herzog ED, Breidenbach et al. Development of sensory, motor and behavioral deficits in the murine model of Sanfilippo Syndrome Type B. *PLoS ONE* 2007; **2**: e772.

5 Fu H, DiRosario J, Kang L, Muenzer J, McCarty DM. Restoration of central nervous system α-N-acetylglucosaminidase activity and therapeutic benefits in mucopolysaccharidosis IIIB mice by a single intracisternal recombinant adeno-associated viral type 2 vector delivery. *J Gene Med* 2010; **12**: 624–633.

6 Cressant A, Desmaris N, Verot L, Bréjot T, Froissart R, Vanier MT et al. Improved behavior and neuropathology in the mouse model of Sanfilippo type IIIB disease after adeno-associated virus-mediated gene transfer in the striatum. *J Neurosci* 2004; **24**: 10229–10239.

7 Ellinwood NM, Ausseil J, Desmaris N, Bigou S, Liu S, Jens JK et al. Safe, efficient, and reproducible gene therapy of the brain in the Dog models of Sanfilippo and Hurler syndromes. *Mol Ther* 2011; **19**: 251–259.

8 Liu G, Martins I, Wemmie JA, Chiorini JA, Davidson BL. Functional correction of CNS phenotypes in a lysosomal storage disease model using adeno-associated virus type 4 vectors. *J Neurosci* 2005; **25**: 9321–9327.

9 Heuer GG, Passini MA, Jiang K, Parente MK, Lee VM-Y, Trojanowski JQ et al. Selective neurodegeneration in murine mucopolysaccharidosis VII is progressive and reversible. *Ann Neurol* 2002; **52**: 762–770.

10 Passini MA, Wolfe JH. Widespread gene delivery and structure-specific patterns of expression in the brain after intraventricular injections of neonatal mice with an adeno-associated virus vector. *J Virol* 2001; **75**: 12382–12392.

11 Passini MA, Watson DJ, Vite CH, Landsburg DJ, Feigenbaum AL, Wolfe JH. Intraventricular brain injection of adeno-associated virus type 1 (AAV1) in neonatal mice results in complementary patterns of neuronal transduction to AAV2 and total long-term correction of storage lesions in the brains of beta-glucuronidase-deficient mice. *J Virol* 2003; **77**: 7034–7040.

12 Sanchez CE, Tierney TS, Gale JT, Alavian KN, Sahin A, Lee J-S et al. Recombinant adeno-associated virus type 2 pseudotypes: comparing safety, specificity, and transduction efficiency in the primate striatum. *J Neurosurg* 2011; **114**: 672–680.

13 Davidson BL, Stein CS, Heth JA, Martins I, Kotin RM, Derksen TA et al. Recombinant adeno-associated virus type 2, 4, and 5 vectors: transduction of variant cell types and regions in the mammalian central nervous system. *Proc Natl Acad Sci USA* 2000; **97**: 3428–3432.

14 Zincarelli C, Soltys S, Rengo G, Rabinowitz JE. Analysis of AAV serotypes 1–9 mediated gene expression and tropism in mice after systemic injection. *Mol Ther* 2008; **16**: 1073–1080.

15 Watson DJ, Passini MA, Wolfe JH. Transduction of the choroid plexus and ependyma in neonatal mouse brain by vesicular stomatitis virus glycoprotein-pseudotyped lentivirus and adeno-associated virus type 5 vectors. *Hum Gene Ther* 2005; **16**: 49–56.

16 Burger C, Gorbatyuk OS, Velardo MJ, Peden CS, Williams P, Zolotukhin S et al. Recombinant AAV viral vectors pseudotyped with viral capsids from serotypes 1, 2, and 5 display differential efficiency and cell tropism after delivery to different regions of the central nervous system. *Mol Ther* 2004; **10**: 302–317.

17 Daly TM, Vogler C, Levy B, Haskins ME, Sands MS. Neonatal gene transfer leads to widespread correction of pathology in a murine model of lysosomal storage disease. *Proc Natl Acad Sci USA* 1999; **96**: 2296–2300.

18 Broekman MLD, Comer LA, Hyman BT, Sena-Esteves M. Adeno-associated virus vectors serotyped with AAV8 capsid are more efficient than AAV-1 or -2 serotypes for widespread gene delivery to the neonatal mouse brain. *Neuroscience* 2006; **138**: 501–510.

19 Gliddon BL, Hopwood JJ. Enzyme-replacement therapy from birth delays the development of behavior and learning problems in mucopolysaccharidosis type IIIA mice. *Pediatr Res* 2004; **56**: 65–72.

20 Heldermon CD, Qin EY, Ohlemiller KK, Herzog ED, Brown JR, Vogler C et al. Disease correction by combined neonatal intracranial AAV and systemic lentiviral gene therapy in Sanfilippo Syndrome type B mice. *Gene Ther* 2013; **20**: 913–921.

21 Gao G-P, Alvira MR, Wang L, Calcedo R, Johnston J, Wilson JM. Novel adeno-associated viruses from rhesus monkeys as vectors for human gene therapy. *Proc Natl Acad Sci USA* 2002; **99**: 11854–11859.

22 Gao G, Vandenberghe LH, Alvira MR, Lu Y, Calcedo R, Zhou X et al. Clades of adeno-associated viruses are widely disseminated in human tissues. *J Virol* 2004; **78**: 6381–6388.

23 Rabinowitz JE, Rolling F, Li C, Conrath H, Xiao W, Xiao X et al. Cross-packaging of a single adeno-associated virus (AAV) type 2 vector genome into multiple AAV serotypes enables transduction with broad specificity. *J Virol* 2002; **76**: 791–801.

24 Foust KD, Nurre E, Montgomery CL, Hernandez A, Chan CM, Kaspar BK. Intravascular AAV9 preferentially targets neonatal neurons and adult astrocytes. *Nat Biotechnol* 2008; **27**: 59–65.

25 Nonnenmacher M, Weber T. Intracellular transport of recombinant adeno-associated virus vectors. *Gene Ther* 2012; **19**: 649–658.

26 Zinn E, Vandenberghe LH. Adeno-associated virus: fit to serve. *Curr Opin Virol* 2014; **8C**: 90–97.

27 Chen YH, Claflin K, Geoghegan JC, Davidson BL. Sialic acid deposition impairs the utility of AAV9, but not peptide-modified AAVs for brain gene therapy in a mouse model of lysosomal storage disease. *Mol Ther* 2012; **20**: 1393–1399.

28 Gray SJ, Nagabhushan Kalburgi S, McCown TJ, Jude Samulski R. Global CNS gene delivery and evasion of anti-AAV-neutralizing antibodies by intrathecal AAV administration in non-human primates. *Gene Ther* 2013; **20**: 450–459.

29 Cucchiarini M, Ren XL, Perides G, Terwilliger EF. Selective gene expression in brain microglia mediated via adeno-associated virus type 2 and type 5 vectors. *Gene Ther* 2003; **10**: 657–667.

30 Cearley CN, Wolfe JH. Transduction characteristics of adeno-associated virus vectors expressing cap serotypes 7, 8, 9, and Rh10 in the mouse brain. *Mol Ther* 2006; **13**: 528–537.

31 Schmidt M, Chiorini JA. Gangliosides are essential for bovine adeno-associated virus entry. *J Virol* 2006; **80**: 5516–5522.

32 Sondhi D, Hackett NR, Peterson DA, Stratton J, Baad M, Travis KM et al. Enhanced survival of the LINCL mouse following CLN2 gene transfer using the rh.10 Rhesus Macaque-derived adeno-associated virus vector. *Mol Ther* 2006; **15**: 481–491.

33 Cachón-González MB, Wang SZ, Lynch A, Ziegler R, Cheng SH, Cox TM. Effective gene therapy in an authentic model of Tay-Sachs-related diseases. *Proc Natl Acad Sci USA* 2006; **103**: 10373–10378.

34 Haurigot V, Marcó S, Ribera A, Garcia M, Ruzo A, Villacampa P *et al*. Whole body correction of mucopolysaccharidosis IIIA by intracerebrospinal fluid gene therapy. *J Clin Invest* 2013; **123**: 3254–3271.

35 Kumar KR, Djarmati-Westenberger A, Grünewald A. Genetics of Parkinson's disease. *Semin Neurol* 2011; **31**: 433–440.

36 Yamanaka K, Chun SJ, Boillee S, Fujimori-Tonou N, Yamashita H, Gutmann DH *et al*. Astrocytes as determinants of disease progression in inherited amyotrophic lateral sclerosis. *Nat Neurosci* 2008; **11**: 251–253.

37 Zhang H, Yang B, Mu X, Ahmed SS, Su Q, He R *et al*. Several rAAV vectors efficiently cross the blood–brain barrier and transduce neurons and astrocytes in the neonatal mouse central nervous system. *Mol Ther* 2011; **19**: 1440–1448.

38 Gray SJ, Matagne V, Bachaboina L, Yadav S, Ojeda SR, Samulski RJ. Preclinical differences of intravascular AAV9 delivery to neurons and glia: a comparative study of adult mice and nonhuman primates. *Mol Ther* 2011; **19**: 1058–1069.

39 Yang B, Li S, Wang H, Guo Y, Gessler DJ, Cao C *et al*. Global CNS transduction of adult mice by intravenously delivered rAAVrh.8 and rAAVrh.10 and nonhuman primates by rAAVrh.10. *Mol Ther* 2014; **22**: 1299–1309.

40 Ribera A, Haurigot V, Garcia M, Marcó S, Motas S, Villacampa P *et al*. Biochemical, histological and functional correction of mucopolysaccharidosis Type IIIB by intra-cerebrospinal fluid gene therapy. *Hum Mol Genet* 2015; **24**: 2078–2095.

41 Petrs-Silva H, Dinculescu A, Li Q, Min S-H, Chiodo V, Pang J-J *et al*. High-efficiency transduction of the mouse retina by tyrosine-mutant AAV serotype vectors. *Mol Ther*. 2009; **17**: 463–471.

42 Gabriel N, Hareendran S, Sen D, Gadkari RA, Sudha G, Selot R *et al*. Bioengineering of AAV2 capsid at specific serine, threonine, or lysine residues improves its transduction efficiency in vitro and in vivo. *Hum Gene Ther Methods* 2013; **24**: 80–93.

43 Sen D, Gadkari RA, Sudha G, Gabriel N, Kumar YS, Selot R *et al*. Targeted modifications in adeno-associated virus serotype 8 capsid improves its hepatic gene transfer efficiency in vivo. *Hum Gene Ther Methods* 2013; **24**: 104–116.

44 Martini SV, da Silva AL, Ferreira D, Gomes K, Ornellas FM, Lopes-Pacheco M *et al*. Single tyrosine mutation in AAV8 vector capsid enhances gene lung delivery and does not alter lung morphofunction in mice. *Cell Physiol Biochem* 2014; **34**: 681–690.

45 Zolotukhin S, Potter M, Zolotukhin I, Sakai Y, Loiler S, Fraites TJ Jr *et al*. Production and purification of serotype 1, 2, and 5 recombinant adeno-associated viral vectors. *Methods* 2002; **28**: 158–167.

46 Marsh J, Fensom AH. 4-Methylumbelliferyl alpha-N-acetylglucosaminidase activity for diagnosis of Sanfilippo B disease. *Clin Genet* 1985; **27**: 258–262.

47 Heldermon CD, Ohlemiller KK, Herzog ED, Vogler C, Qin E, Wozniak DF *et al*. Therapeutic efficacy of bone marrow transplant, intracranial AAV-mediated gene therapy, or both in the mouse model of MPS IIIB. *Mol Ther* 2010; **18**: 873–880.